This manuscript has been authored by UT-Battelle, LLC under Contract No. DE-AC05-00OR22725 with the U.S. Department of Energy. The United States Government retains and the publisher, by accepting the article for publication, acknowledges that the United States Government retains a non-exclusive, paid-up, irrevocable, world-wide license to publish or reproduce the published form of this manuscript, or allow others to do so, for United States Government purposes. The Department of Energy will provide public access to these results of federally sponsored research in accordance with the DOE Public Access Plan (http://energy.gov/downloads/doe-public-access-plan).

Large dielectric constant, high acceptor density, and deep electron traps in perovskite solar cell material $CsGeI_3$

Wenmei Ming[1],[†] Hongliang Shi[1,2],[†] and Mao-Hua Du[1]

[1]Materials Science & Technology Division and Center for Radiation Detection Materials and Systems, Oak Ridge National Laboratory, Oak Ridge, TN 37831, USA

[2]Key Laboratory of Micro-Nano Measurement-Manipulation and Physics (Ministry of Education), School of Physics and Nuclear Energy Engineering, Beihang University, Beijing 100191, China

AUTHOR INFORMATION

Corresponding Author

Mao-Hua Du (mhdu@ornl.gov)

[†] These authors contribute equally to this work.

ABSTRACT Many metal halides that contain cations with ns^2 electronic configuration have recently been discovered as high-performance optoelectronic materials. In particular, solar cells based on lead halide perovskites have shown great promise as evidenced by the rapid increase of the power conversion efficiency. In this paper, we show density functional theory calculations of electronic structure and dielectric and defect properties of $CsGeI_3$ (a lead-free halide perovskite material). The potential of $CsGeI_3$ as a solar cell material is assessed based on its intrinsic properties. We find anomalously large Born effective charges and a large static dielectric constant dominated by lattice polarization, which should reduce carrier scattering, trapping, and recombination by screening charged defects and impurities. Defect calculations show that $CsGeI_3$ is a p-type semiconductor and its hole density can be modified by varying the chemical potentials of the constituent elements. Despite the reduction of long-range Coulomb attraction by strong screening, the iodine vacancy in $CsGeI_3$ is found to be a deep electron trap due to the short-range potential, i.e., strong Ge-Ge covalent bonding, which should limit electron transport efficiency in p-type $CsGeI_3$. This is in contrast to the shallow iodine vacancies found in several Pb and Sn halide perovskites (e.g., $CH_3NH_3PbI_3$, $CH_3NH_3SnI_3$, and $CsSnI_3$). The low-hole-density $CsGeI_3$ may be a useful solar absorber material but the presence of the low-energy deep iodine vacancy may significantly reduce the open circuit voltage of the solar cell. On the other hand, $CsGeI_3$ may be used as an efficient hole transport material in solar cells due to its small hole effective mass, the absence of low-energy deep hole traps, and the favorable band offset with solar absorber materials such as dye molecules and $CH_3NH_3PbI_3$.

I. Introduction

Halides are usually ionic compounds which have large band gaps and are prone to defect formation due to their soft lattices. However, some metal halides that contain ns^2 ions (ions with outer electron configuration of ns^2, e.g., Tl^+, Pb^{2+}, Bi^{3+} and Sn^{2+}) have significant covalency to enable efficient carrier transport and have relatively small band gaps (due to the relatively high electronegativity of the ns^2 ions) for various optoelectronic applications such as photovoltaics (PV) and photodetection. The mixed ionic-covalent character of these halides leads to strong lattice polarization and a large static dielectric constant, which provides strong screening to charged defects and impurities, thereby suppressing carrier scattering and trapping.[1, 2] Among halides that contain ns^2 cations, Tl^+ and Pb^{2+} based halides have received most of the attention. The electron and hole diffusion lengths in single-crystal and polycrystalline $CH_3NH_3PbI_3$ exceed 100 μm and 1μm, respectively.[3-6] The power conversion efficiency (PCE) of the halide perovskite solar cells has exceeded 20%, which is close to the PCE of CdTe and CIGS thin-film solar cells.[7] Single-crystal TlBr has a large electron mobility-lifetime product (6×10^{-3} cm^2/V) comparable to that of CdTe.[8, 9] Tl_6SeI_4,[10] Tl_6SI_4,[11] and $CsPbBr_3$[12] have also been reported to have good carrier transport properties. TlBr, Tl_6SeI_4, Tl_6SI_4, $CsPbBr_3$, and $CH_3NH_3PbI_3$ have all been investigated as radiation or photodetection materials.[8-11, 13-15] Replacing the ns^2 ions with other isovalent ions (such as replacing Pb^{2+} in halide perovskites by alkali earth metals) usually leads to much larger band gaps and effective masses.[16, 17]

One of the problems of Tl^+ and Pb^{2+} based halides is the toxicity of Tl and Pb, which is a challenge to the wide-spread use of these materials. The Bi^{3+} and Sb^{3+} based halides have the advantage of having low toxicity but often have crystal structures of reduced dimensionality (due

to the large oxidation state of Bi^{3+} and Sb^{3+} and the resulting high anion/cation ratio), which leads to anisotropic structural, electronic, and dielectric properties.[18-21]

Tin and germanium iodide perovskites ($CsSnI_3$,[22, 23] $CH_3NH_3SnI_3$,[24, 25] $CsGeI_3$,[26] and $CH_3NH_3GeI_3$,[26]) are the obvious candidates in the search for Pb-free halide perovskite solar cell materials. Compared to lead iodide perovskites ($APbI_3$), the tin/germanium iodide perovskites ($ASnI_3$/$AGeI_3$) have stronger anti-bonding character near the valence band maximum (VBM) due to the more active Sn 5s/Ge 4s lone pairs than the Pb 6s lone pair. The Sn 5s/Ge 4s band below the valence band hybridizes significantly with the I-5p-states in the valence band; their anti-bonding states reside near the VBM, which makes it easy to create holes at the VBM, effectively oxidizing Sn^{2+}/Ge^{2+}. The resulting large hole density in tin/germanium iodide perovskites often leads to metallic conductivity and short circuit behavior of the solar cell.[22, 26, 27 28] Semiconducting tin and germanium iodide perovskites (such as $CH_3NH_3SnI_3$) can also be made by synthesis from solution.[26, 29, 30] However, the solar cells that employ $CH_3NH_3SnI_3$, $CH_3NH_3GeI_3$, and $CsGeI_3$ as solar absorber materials have so far shown much lower PCE than those of lead halide perovskites.[24-27] $CsSnI_3$ has also been used as a hole transport material (HTM) in dye-sensitized TiO_2 solar cells, which show PCE up to 10.2%.[23]

$CsGeI_3$ has been investigated as a solar absorber material[26] but not yet as a hole transport material. In contrast to $CsPbI_3$ and $CsSnI_3$, which have instability towards the formation of yellow phases (with 1D chain structures and large band gaps) at room temperature,[29] $CsGeI_3$ has a 3D perovskite structure with a small rhombohedral distortion (space group R3m) (see Figure 1) and does not encounter crystal phase transitions in low-temperature solution growth.[30] $CsGeI_3$ has a band gap of 1.6 eV at room temperature, suitable for PV applications.[30] The calculated band structure of $CsGeI_3$ shows dispersive valence band, favorable for hole transport.[30] The

VBM of $CsGeI_3$ (i.e., -5.1 eV[26] relative to the vacuum level) is lower than those of $CsSnI_3$ and $CH_3NH_3SnI_3$ (i.e., -4.95 eV[23] and -4.6 eV[27], respectively) and is closer to the VBM of the typical HTM (-5.2 eV).[27, 31] Thus, compared with $CsSnI_3$ and $CH_3NH_3SnI_3$, $CsGeI_3$, when used as a solar absorber, has the advantage of making better Ohmic contact (for hole transport) with the HTM/Au electrode in the solar cell.

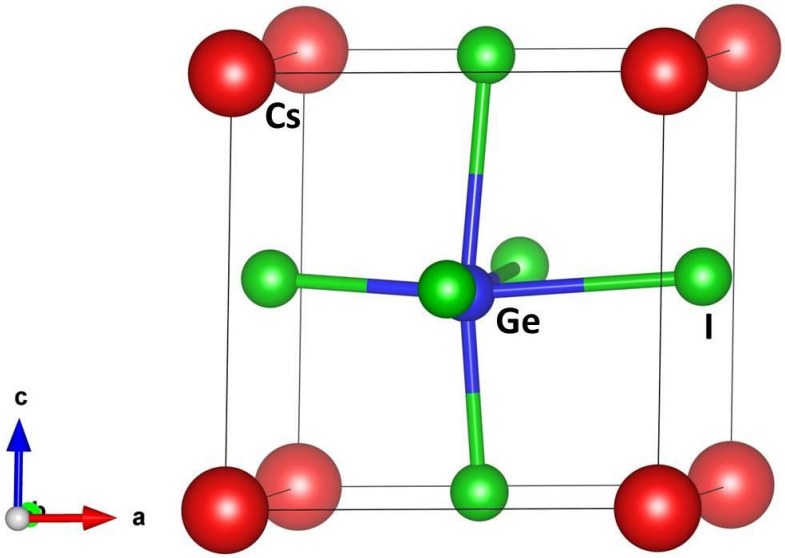

Figure 1. Structure of $CsGeI_3$.

In this paper, we show DFT calculations of electronic structure and dielectric and defect properties of $CsGeI_3$. Similar to other halide perovskites that contain ns^2 ions, $CsGeI_3$ has small electron and hole effective masses, strongly enhanced Born effective charges, and a large static dielectric constant dominated by lattice polarization. Defect calculations show that V_{Ge} and V_{Cs} are important native acceptors while V_I is the most important donor defect. $CsGeI_3$ is found to be a p-type semiconductor; the Fermi level and the hole density can be tuned by varying the chemical potentials of the constituent elements. V_I is predicted to be a deep electron trap and non-radiative recombination center, in contrast to the shallow iodine vacancies found in $CH_3NH_3PbI_3$, $CH_3NH_3SnI_3$, and $CsSnI_3$.[2, 28, 32-34] Defect chemistry in $CsGeI_3$ is discussed in relation to other

halide perovskite materials. The deep donor V_I in $CsGeI_3$ is consistent with the measured low open circuit voltage (V_{OC})[26] and should be a challenge to the development of $CsGeI_3$ as a solar absorber material. However, $CsGeI_3$ may be used as a hole transport material in solar cells due to its small hole effective masses, the absence of low-energy deep hole traps, and the favorable band offset between $CsGeI_3$ and solar absorber materials such as dye molecules and $CH_3NH_3PbI_3$.

II. Computational Methods

All calculations were performed based on density functional theory. Born effective charges and dielectric constants were calculated using Perdew, Burke, and Ernzerhof (PBE)[35] generalized gradient approximation (GGA) without spin-orbit coupling (SOC). Defect formation energies are given by:

$$\Delta H = (\mathrm{E}_D - \mathrm{E}_h) - \sum_i n_i(\mu_i + \mu_i^{ref}) + q(\varepsilon_{VBM} + \varepsilon_f), \quad (1)$$

where E_D and E_h are the total energies of the defect-containing and the host (i.e. defect-free) supercells. Formation of a defect involves exchange of atoms with their respective chemical reservoirs. The second term in Eq.(1) represents the change in energy due to such exchange of atoms, where n_i is the difference in the number of atoms for the *i'*th atomic species between the defect-containing and defect-free supercells. μ_i is the relative chemical potential for the *i'*th atomic species, referenced to its bulk μ_i^{ref}. The third term in Eq.(1) represents the change in energy due to exchange of electrons with its reservoir. ε_{VBM} is the energy of the VBM and ε_f is the Fermi energy relative to the VBM. The transition level of a defect, $\varepsilon(q/q')$, corresponding to

a change in its charge state between q and q', is given by the Fermi level, at which the formation energies, $\Delta H(q)$ and $\Delta H(q')$, for charge states q and q' are equal to each other:

$$\varepsilon(q/q') = [\Delta H(q) - \Delta H(q')]/(q' - q). \quad (2)$$

The defect formation energies were calculated using PBE functionals with the VBM and the conduction band minimum (CBM) from the PBE calculation corrected using hybrid density functional calculations. The band gap of $CsGeI_3$ calculated using PBE functionals including the SOC is 0.79 eV. The Heyd-Scuseria-Ernzerhof (HSE) hybrid functional calculation including the SOC was used to correct the band gap. The fraction of the Fock exchange was adjusted to 45% to produce a band gap of 1.57 eV, in good agreement with the experimental value of 1.6 eV.[30] The shallow defect levels, which have mainly the character of bulk electronic states, were first calculated using PBE functionals and then were shifted with their respective HSE-corrected band edges, while the deep levels, which are highly localized, were not corrected since they are not expected to move following the band gap correction.[36, 37, 38] Corrections to the defect formation energy due to potential alignment (between the host and a charged defect supercell), band filling effects, and image charge were applied wherever appropriate.[39] We used a 2×2×2 supercell (135 atoms if defect free) and a 2×2×2 k-point mesh for the calculations of defect formation energies and defect levels. The SOC was not included in the total energy and the structural relaxation calculations of the defect systems. The experimental lattice parameters (space group R3m, a = b = c = 5.983 Å and α = β = γ = 88.61°) were used in all calculations.[40] Using theoretical or experimental lattice parameters should make little differences in defect levels and formation energies,[38] which involve only the calculations of energy differences rather than absolute energies.

The lattice part of the static dielectric constant, ε_{ion}, was calculated using PBE functionals; the electronic part, ε_{∞}, was calculated using HSE hybrid functionals with 45% Fock exchange (which corrects the PBE band gap error) because ε_{∞} is sensitive to the band gap.

The PBE and HSE calculations were performed using projector augmented wave method (PAW)[41] as implemented in the VASP code.[42, 43] The cut-off energy for the plane waves was set at 310 eV and all forces were minimized to < 0.02 eV/Å in the structural relaxation calculations. For the calculations of Born effective charges and the ionic part of the static dielectric constant, which require more stringent force accuracy, a higher cutoff energy of 400 eV and a tighter force convergence criterion (< 0.01 eV/Å) were used.

III. Results and Discussion

The Born effective charge is a measure of how lattice polarization develops with atomic displacements. Halides that contain ns^2 cations typically exhibit mixed ionic-covalent character, which gives rise to anomalously high Born effective charges and strong lattice polarization.[1, 2, 20, 44, 45] Table I shows the calculated Born effective charges of $CsGeI_3$. The Born effective charge of Ge is more than doubled and those of I are more than quadrupled from their nominal ionic charges along the Ge-I bond directions due to the mixed ionic-covalent Ge-I bonds in $CsGeI_3$. The large Born effective charges lead to strong lattice polarization as evidenced by the calculated large static dielectric constant dominated by the ionic contribution (Table II). The calculated static dielectric constant (18.6) of $CsGeI_3$ is large compared to semiconductors with similar band gaps. A large static dielectric constant provides strong screening to the charged impurities and defects, thereby suppressing the charge trapping and recombination. This is an important

characteristic related to the efficient carrier transport in halides that contain ns^2 cations.[1, 2, 20, 44-46] The calculated static dielectric constant of $CsGeI_3$ is close to that calculated for $CH_3NH_3PbI_3$, ~21.7, (without considering the response by the dipolar CH_3NH_3 molecules).[2] The experimentally measured static dielectric constant of $CH_3NH_3PbI_3$ is 60-70.[31, 47-49] The free-rotating dipolar CH_3NH_3 molecules make a significant contribution to the total static dielectric constant of $CH_3NH_3PbI_3$.

Table I. DFT-PBE-calculated Born effective charges for Ge and I in $CsGeI_3$. The lattice vector a of $CsGeI_3$ is aligned with the x axis in Cartesian coordinates. Since the rhombohedral $CsGeI_3$ is only slightly distorted from the cubic structure, the lattice vectors b and c are nearly aligned with the y and the z axes, respectively. I(x), I(y), and I(z) denote the three iodine ions with Ge-I bonds aligned approximately with x, y, and z axes. Note that the nominal ionic charges of Ge and I are +2 and -1, respectively.

Ge	I (x)	I (y)	I (z)
Z_{xx} = 4.32	Z_{xx} = -4.53	Z_{xx} = -0.64	Z_{xx} = -0.64
Z_{yy} = 4.34	Z_{yy} = -0.65	Z_{yy} = -4.54	Z_{yy} = -0.64
Z_{zz} = 4.35	Z_{zz} = -0.65	Z_{zz} = -0.65	Z_{zz} = -4.54

Table II. Calculated static dielectric constant (ε_{st}) of $CsGeI_3$ and the electronic (ε_{∞}) and the ionic (ε_{ion}) contributions to the static dielectric constant. The results shown here are 1/3 of the trace of the dielectric tensors.

ε_{∞}	ε_{ion}	ε_{st}
5.0	13.6	18.6

We performed total energy calculations for $CsGeI_3$ and competing phases to construct the phase diagram. To obtain stable growth of $CsGeI_3$ without the formation of other completing phases (e.g., CsI, GeI_2, GeI_4, and Cs_2I_8), the relative chemical potentials of Tl, Se, and I in Eq. 1 must be constrained to meet the following conditions.

$$
\begin{aligned}
&\mu_{\mathrm{Cs}} + \mu_{\mathrm{Ge}} + 3\mu_{\mathrm{I}} = \Delta H(\mathrm{CsGeI_3}) \\
&\mu_{\mathrm{Cs}} \le 0 \\
&\mu_{\mathrm{Ge}} \le 0 \\
&\mu_{\mathrm{I}} \le 0 \\
&\mu_{\mathrm{Cs}} + \mu_{\mathrm{I}} \le \Delta H(\mathrm{CsI}) \\
&\mu_{\mathrm{Ge}} + 2\mu_{\mathrm{I}} \le \Delta H(\mathrm{GeI_2}) \\
&\mu_{\mathrm{Ge}} + 4\mu_{\mathrm{I}} \le \Delta H(\mathrm{GeI_4}) \\
&2\mu_{\mathrm{Cs}} + 8\mu_{\mathrm{I}} \le \Delta H(\mathrm{Cs_2I_8}),
\end{aligned}
\tag{1}
$$

where $\Delta H(\mathrm{CsGeI_3})$, $\Delta H(\mathrm{CsI})$, $\Delta H(\mathrm{GeI_2})$, $\Delta H(\mathrm{GeI_4})$, and $\Delta H(\mathrm{Cs_2I_8})$ are the enthalpies of formation (per formula unit) of $\mathrm{CsGeI_3}$, CsI, $\mathrm{GeI_2}$, $\mathrm{GeI_4}$, and $\mathrm{Cs_2I_8}$, respectively. The chemical potential ranges for single-phase $\mathrm{CsGeI_3}$ are shown in Fig. 2 along with those for other competing phases.

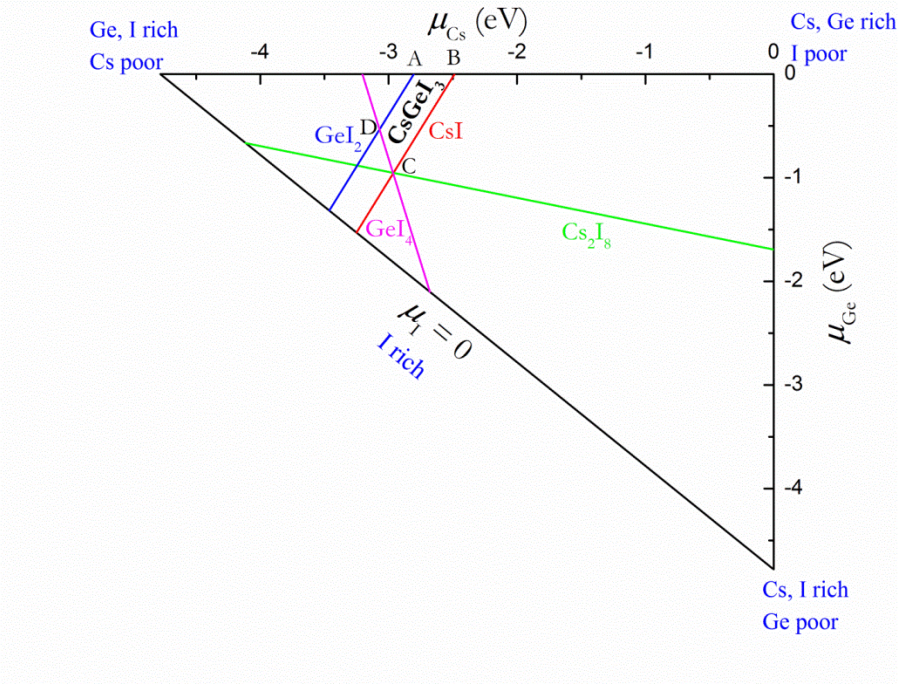

Figure 2. Calculated ranges of chemical potentials for CsGeI3 and its competing phases under thermal equilibrium. The polygon ABCD is the region where $\mathrm{CsGeI_3}$ is stable without forming other phases.

Figure 3 shows the native defect formation energies calculated using chemical potentials corresponding to points A, B, C, and D in Figure 2, which are on the boundaries of the stable $CsGeI_3$ region. The low-energy native defects play an important role in charge carrier transport. As can be seen in Figure 3, the most important native defects in $CsGeI_3$ are vacancies, i.e., Ge and Cs vacancies (V_{Ge} and V_{Cs}) as acceptors and the iodine vacancy (V_I) as a donor. Compared to vacancies, the formation of interstitials is usually energetically less favorable in the close-packed perovskite structure. The antisite involving a cation on the anion site or an anion on the cation site is also likely to cause large formation energy in materials with relatively high ionicity. Therefore, vacancies are usually the most common defects in halides. We note that recent DFT calculations predicted that methylammonium (MA) interstitial MA_i in $MAPbI_3$ and Sn_I (Sn on I site) in $CsSnI_3$ are low-energy native donor defects, even more stable than halogen vacancy defects.[28, 32] These results are highly unusual. In $CsGeI_3$, we find that Cs_i and Ge_I both have relatively high formation energies regardless of the chemical potentials.

At the Ge-poor and I-rich limit (point C in Fig. 2), V_{Ge} has very low formation energy, followed by V_{Cs}. Both are shallow acceptors as shown in Fig. 4 and can easily produce free holes in $CsGeI_3$. There is no native donor defect to effectively compensate these native acceptor defects. The Fermi level should be near the VBM. Under this condition, $CsGeI_3$ could be a degenerate semiconductor, acting more like a metal than a semiconductor. The high hole conductivity may lead to metallic conductivity in $CsGeI_3$ and the short circuit behavior of the solar cell.

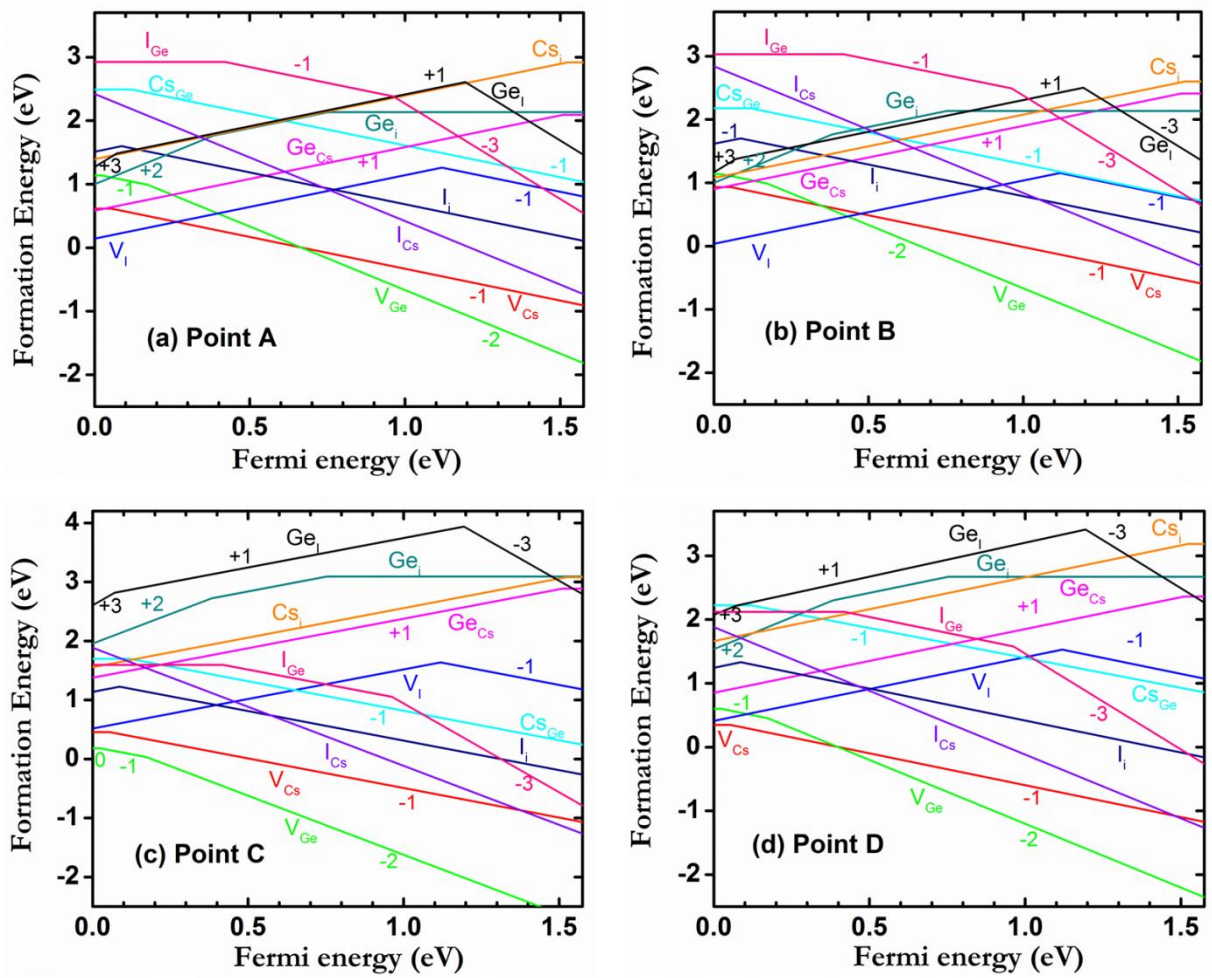

Figure 3. Calculated formation energies of native defects in $CsGeI_3$ using chemical potentials corresponding to points A (a), B (b), C (c), and D (d) in Figure 2. Slopes of the formation energy lines indicate the charge states of the defects. A transition level is where the slope changes.

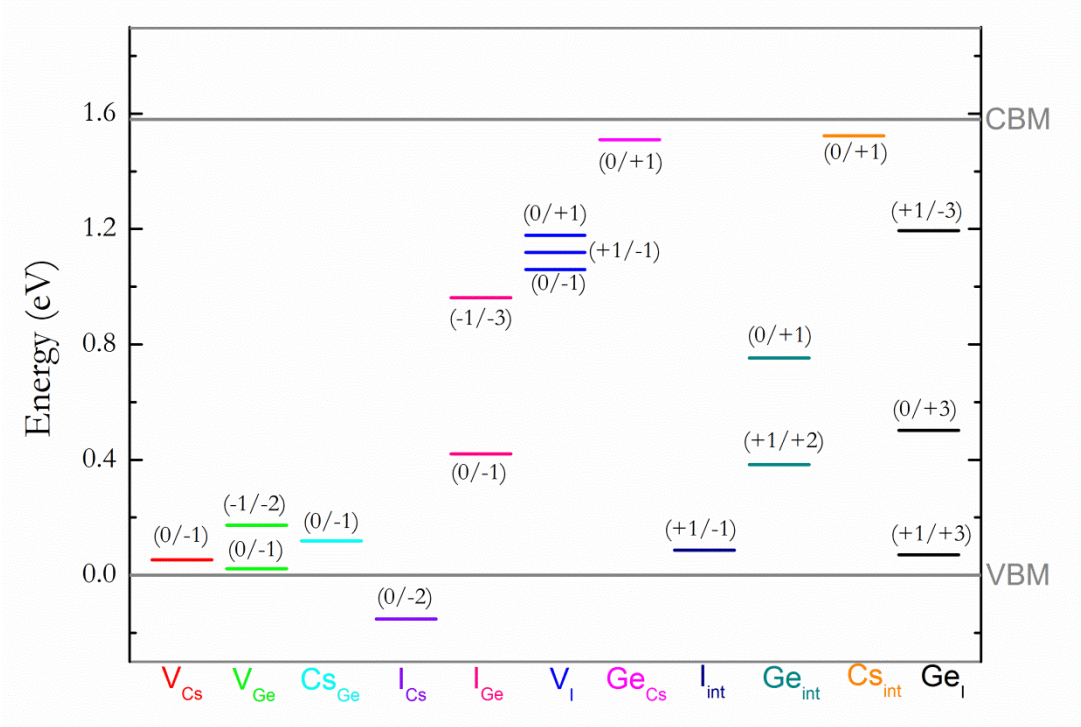

Figure 4. Calculated charge transition levels for native defects in $CsGeI_3$.

Under the Ge-rich, Cs-rich, and I-poor limit (point B in Fig. 2), the concentrations of V_{Ge} and V_{Cs} are reduced while V_I becomes more abundant. The formation energy lines of V_I and V_{Ge} cross at ε_v + 0.43 eV [Fig. 3(b)]. The Fermi level should be located near this crossing point, resulting in p-type semiconducting $CsGeI_3$, which may be used as a p-type solar absorber material. An important result here is that V_I is found to be a deep electron trap and nonradiative recombination center since the calculated (+/0) and (0/-) levels of V_I are both deep inside the band gap as shown in Fig. 4. V_I plays an important role of compensating the shallow native acceptors (V_{Ge} and V_{Cs}) and preventing metallic conductivity, which is necessary for using $CsGeI_3$ as a solar absorber material. On the other hand, V_I, as a deep electron trap, can seriously reduce the electron mobility and lifetime. The presence of the deep donor V_I in $CsGeI_3$ is consistent with the measured low open circuit voltage (V_{OC}) in $CsGeI_3$ solar cells.[26]

The halogen vacancy is an important defect in halides and usually induces deep levels inside the band gap. However, halogen vacancies in TlBr and $CH_3NH_3PbI_3$ are shallow donors,[2, 32, 34, 50] which strongly contribute to the efficient electron transport observed in these halides. The electron trapping energy in the halogen vacancy is determined by the long-range Coulomb attraction and the short-range potential arising from the cation orbital hybridization at the vacancy. The former is more important in ionic compounds while the latter is more important in covalent compounds. Halides usually have significant ionicity. However, in halides that contain ns^2 cations, the static dielectric constant is usually large, which reduces the long-range Coulomb attraction. Thus, the hybridization of the cation orbitals plays an important role in determining the electron trapping energy at a halogen vacancy.[34] This is particularly true for $CsGeI_3$, where a strong covalent bond can form between the two Ge atoms adjacent to the iodine vacancy for trapping electrons. The two Ge ions near V_I^+ is separated by a long distance of 6.36 Å due to the Coulomb repulsion. The addition of one or two electrons creates an energy incentive for the two Ge ions to move closer, resulting in stronger orbital hybridization and a bound state to trap the added electrons. The Ge-Ge distances in V_I^0 and V_I^- are reduced to 2.95 Å and 2.79 Å, respectively. The two Ge ions adjacent to V_I^+ are five-fold coordinated. But in V_I^-, these two Ge ions form a strong Ge-Ge bond as shown in Fig. 5. Each of these two Ge ions retains strong bonding with only two of its neighboring I ions and breaks away from the other three I neighbors. Figure 5 shows the isodensity surface of the partial charge density associated with the localized Ge-Ge bond. Despite the energy cost due to the structural distortion, the formation of the strong Ge-Ge covalent bond significantly lowers the total energy and makes the deep electron trapping energetically favorable. The Sn-Sn and the Pb-Pb bonds in Sn and Pb halide perovskites are

considerably weaker than the Ge-Ge bond. This may explain the deep V_I in $CsGeI_3$ vs. shallow V_I in $CH_3NH_3PbI_3$, $CH_3NH_3SnI_3$, and $CsSnI_3$.

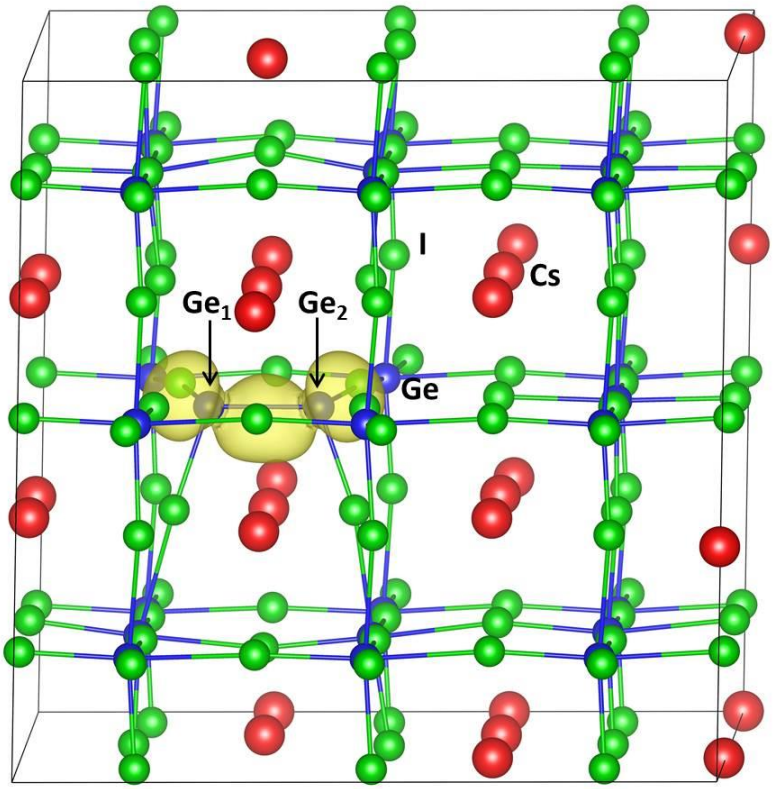

Figure 5. Structure of V_I^-. The two Ge ions (Ge_1 and Ge_2) form a covalent bond. Each of them is coordinated with only two iodine ions. The isodensity surface (0.0035 e/Bohr^3) of the partial charge density associated with the Ge-Ge bond is also shown.

$CsSnI_3$ had been investigated as a hole transport material in dye-sensitized TiO_2 solar cells.[23] However, the VBM and the CBM of $CsGeI_3$ provide better band offset with the dye molecules than those of $CsSnI_3$ as shown in Fig. 6. The CBM of $CsSnI_3$ (-3.62 eV relative to the vacuum level[23]) is slightly lower than the lowest unoccupied molecular orbital (LUMO) of the N719 dye molecules (-3.64 eV[23]); thus, although $CsSnI_3$ can conduct holes, it does not

effectively block electrons. On the other hand, the CBM of $CsGeI_3$ (-3.45 eV[26]) is higher than the LUMO of the N719 dye molecules, thus, providing more reliable rejection of electrons from the dyes. Compared to the VBM of $CsSnI_3$ (-4.92 eV[23]), the VBM of $CsGeI_3$ (-5.1 eV[26]) is closer to the highest occupied molecular orbital (HOMO) of the N719 dye molecule (-6.01 eV[23]), which may lead to higher open circuit voltage while still allowing hole extraction from the dyes. Furthermore, $CsGeI_3$ has small effective masses as shown in Table III and has no low-energy deep native acceptors as shown in Figures 3 and 4. Thus, $CsGeI_3$ may be a potential hole transport material in dye-sensitized TiO_2 solar cells.

$CsGeI_3$ has an optical band gap of 1.6 eV and thus may also absorb photons in a dye-sensitized solar cell. The band alignment diagram (Figure 6) shows that it is energetically favorable for the electrons in the conduction band of $CsGeI_3$ to be transferred to the LUMO of the N719 dye molecule. Importantly, the energy difference between the CBM of $CsGeI_3$ and the LUMO of the N719 dye molecule (0.19 eV) is significantly smaller than the electron trapping energy at the I vacancy (0.4 eV). Thus, it should be more efficient for a photoelectron in $CsGeI_3$ near the $CsGeI_3$/N719 interface to be transferred to the N719 dye molecule than to be trapped by the I vacancy because less phonons need to be emitted for the electron transfer from $CsGeI_3$ to the N719 dye molecules.

From a band alignment point of view, $CsGeI_3$, as a hole transport material, is also compatible with the $CH_3NH_3PbI_3$ solar absorber, which has its VBM and CBM at -5.5 and -3.9 eV, respectively.[31] However, the $CsGeI_3$ hole conductor should probably be avoided in an inverted $CH_3NH_3PbI_3$ solar cell, in which the photons need to pass through the hole conductor before reaching the $CH_3NH_3PbI_3$ solar absorber, because the $CsGeI_3$ solar absorber can absorb

the solar irradiation and lead to energy loss due to its low-energy deep iodine vacancy defect as shown in Figures 3 and 4.

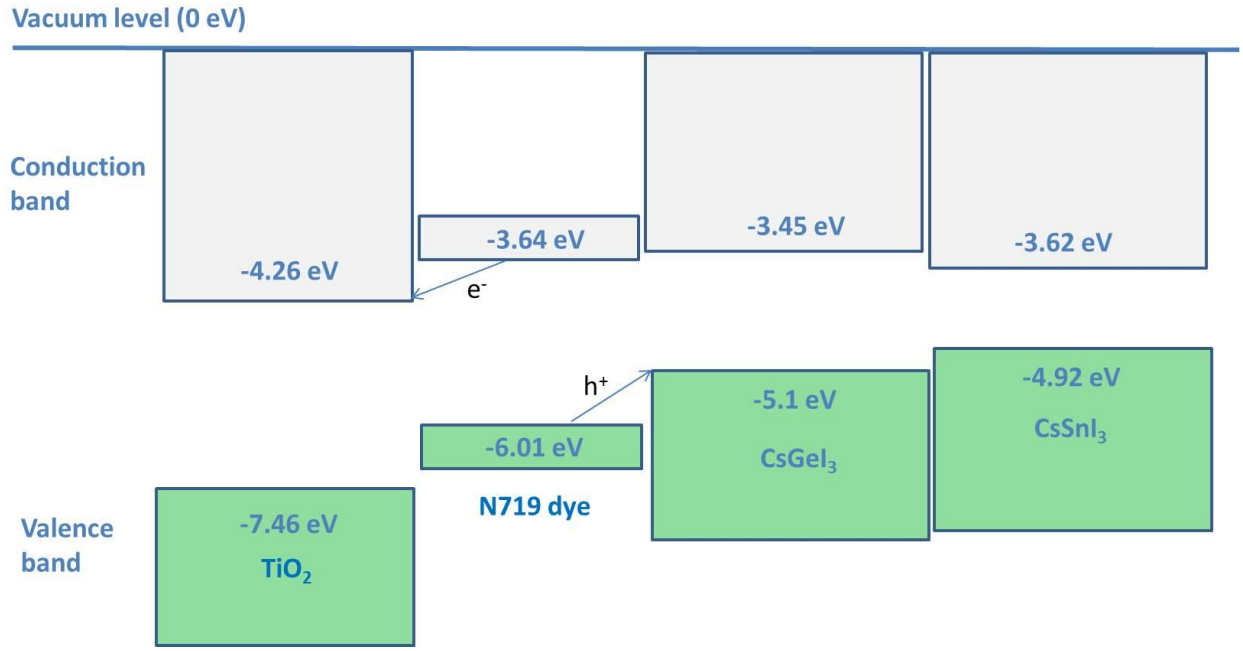

Figure 6. Schematic band alignment diagram of the N719 dye-sensitized TiO_2 solar cell with $CsGeI_3$ or $CsSnI_3$ as the hole transport material. The energy values of the valence and conduction band edges are shown relative to the vacuum level (0 eV).[23, 26] The arrows indicate the electron (e^-) and hole transport (h^+) direction after photoexcitation of e^--h^+ pairs in N719 dye.

Table III. Hole and electron effective masses (m_h and m_e) along different directions in $CsGeI_3$. m_0 is the electron rest mass. The VBM and the CBM are both located at the Z point. The band structure is shown in the Supporting Information.

	Z→L	Z→Γ
m_h/m_0	0.22	0.21
m_e/m_0	0.42	0.21

IV. Conclusion

Density functional calculations are performed to study dielectric and defect properties of $CsGeI_3$. Consistent with other halides that contain ns^2 ions, $CsGeI_3$ exhibits anomalously large Born effective charges and a large static dielectric constant dominated by strong lattice polarization. A large dielectric constant provides strong screening to charged defects and impurities, thereby reducing carrier scattering, trapping, and recombination. The defect calculations show that, (1) under Ge-poor conditions, $CsGeI_3$ should have a high density of the shallow native acceptor Ge vacancy, which can generate high free hole density and may result in metallic conductivity and the short circuit behavior of $CsGeI_3$ solar cells; (2) under Ge-rich conditions, $CsGeI_3$ is a semiconducting material with reduced hole density and conductivity due to the increased concentration of compensating donors, i.e., the iodine vacancy. The semiconducting $CsGeI_3$ may be used as a solar absorber material. However, the iodine vacancy in $CsGeI_3$ is a deep electron trap and nonradiative recombination center due to the strong Ge-Ge covalent bonding, which is in contrast to the shallow iodine vacancies found in several Pb and Sn halide perovskites, e.g., $CH_3NH_3PbI_3$, $CH_3NH_3SnI_3$, and $CsSnI_3$. The presence of the iodine-vacancy-induced deep traps in $CsGeI_3$ should limit the performance of $CsGeI_3$ solar cells. However, $CsGeI_3$ may have high potential to be used as an efficient hole transport material in solar cells due to its small hole effective masses, the absence of low-energy deep hole traps, and the favorable band offset between $CsGeI_3$ and solar absorber materials such as dye molecules and $CH_3NH_3PbI_3$.

Supporting Information:

Calculated band structure of $CsGeI_3$.

Acknowledgment:

This work was supported by the U. S. Department of Energy, Office of Science, Basic Energy Sciences, Materials Sciences and Engineering Division.

REFERENCES

1. M. H. Du and D. J. Singh, *Physical Review B*, 2010, **81**, 045203.
2. M. H. Du, *Journal of Materials Chemistry A*, 2014, **2**, 9091-9098.
3. Q. Dong, Y. Fang, Y. Shao, P. Mulligan, J. Qiu, L. Cao and J. Huang, *Science*, 2015, **347**, 967-970.
4. S. D. Stranks, G. E. Eperon, G. Grancini, C. Menelaou, M. J. P. Alcocer, T. Leijtens, L. M. Herz, A. Petrozza and H. J. Snaith, *Science*, 2013, **342**, 341-344.
5. G. Xing, N. Mathews, S. Sun, S. S. Lim, Y. M. Lam, M. Graetzel, S. Mhaisalkar and T. C. Sum, *Science*, 2013, **342**, 344-347.
6. C. Wehrenfennig, G. E. Eperon, M. B. Johnston, H. J. Snaith and L. M. Herz, *Advanced Materials*, 2014, **26**, 1584-1589.
7. https://www.nrel.gov/ncpv/images/efficiency_chart.jpg).
8. A. V. Churilov, G. Ciampi, H. Kim, L. J. Cirignano, W. M. Higgins, F. Olschner and K. S. Shah, *Ieee Transactions on Nuclear Science*, 2009, **56**, 1875-1881.
9. A. V. Churilov, G. Ciampi, H. Kim, W. M. Higgins, L. J. Cirignano, F. Olschner, V. Biteman, M. Minchello and K. S. Shah, *Journal of Crystal Growth*, 2010, **312**, 1221-1227.
10. S. Johnsen, Z. Liu, J. A. Peters, J.-H. Song, S. Nguyen, C. D. Malliakas, H. Jin, A. J. Freeman, B. W. Wessels and M. G. Kanatzidis, *Journal of the American Chemical Society*, 2011, **133**, 10030-10033.
11. S. L. Nguyen, C. D. Malliakas, J. A. Peters, Z. Liu, J. Im, L.-D. Zhao, M. Sebastian, H. Jin, H. Li, S. Johnsen, B. W. Wessels, A. J. Freeman and M. G. Kanatzidis, *Chemistry of Materials*, 2013, **25**, 2868-2877.
12. C. C. Stoumpos, C. D. Malliakas, J. A. Peters, Z. Liu, M. Sebastian, J. Im, T. C. Chasapis, A. C. Wibowo, D. Y. Chung, A. J. Freeman, B. W. Wessels and M. G. Kanatzidis, *Crystal Growth & Design*, 2013, **13**, 2722-2727.
13. R. Dong, Y. Fang, J. Chae, J. Dai, Z. Xiao, Q. Dong, Y. Yuan, A. Centrone, X. C. Zeng and J. Huang, *Advanced Materials*, 2015, **27**, 1912-1918.
14. Y. Yuan and J. Huang, *Advanced Optical Materials*, 2016, **4**, 264-270.

15. H. Wei, Y. Fang, P. Mulligan, W. Chuirazzi, H.-H. Fang, C. Wang, B. R. Ecker, Y. Gao, M. A. Loi, L. Cao and J. Huang, *Nat Photon*, 2016, **10**, 333-339.
16. T. J. Jacobsson, M. Pazoki, A. Hagfeldt and T. Edvinsson, *The Journal of Physical Chemistry C*, 2015, **119**, 25673-25683.
17. M. Pazoki, T. J. Jacobsson, A. Hagfeldt, G. Boschloo and T. Edvinsson, *Physical Review B*, 2016, **93**, 144105.
18. R. E. Brandt, R. C. Kurchin, R. L. Z. Hoye, J. R. Poindexter, M. W. B. Wilson, S. Sulekar, F. Lenahan, P. X. T. Yen, V. Stevanović, J. C. Nino, M. G. Bawendi and T. Buonassisi, *The Journal of Physical Chemistry Letters*, 2015, **6**, 4297-4302.
19. H. Shi, W. Ming and M.-H. Du, *Physical Review B*, 2016, **93**, 104108.
20. M.-H. Du and D. J. Singh, *Physical Review B*, 2010, **82**, 045203.
21. B. Saparov, F. Hong, J.-P. Sun, H.-S. Duan, W. Meng, S. Cameron, I. G. Hill, Y. Yan and D. B. Mitzi, *Chemistry of Materials*, 2015, **27**, 5622-5632.
22. I. Chung, J.-H. Song, J. Im, J. Androulakis, C. D. Malliakas, H. Li, A. J. Freeman, J. T. Kenney and M. G. Kanatzidis, *Journal of the American Chemical Society*, 2012, **134**, 8579-8587.
23. I. Chung, B. Lee, J. He, R. P. H. Chang and M. G. Kanatzidis, *Nature*, 2012, **485**, 486-489.
24. F. Hao, C. C. Stoumpos, D. H. Cao, R. P. H. Chang and M. G. Kanatzidis, *Nat Photon*, 2014, **8**, 489-494.
25. N. K. Noel, S. D. Stranks, A. Abate, C. Wehrenfennig, S. Guarnera, A. A. Haghighirad, A. Sadhanala, G. E. Eperon, S. K. Pathak, M. B. Johnston, A. Petrozza, L. M. Herz and H. J. Snaith, *Energy & Environmental Science*, 2014, **7**, 3061-3068.
26. T. Krishnamoorthy, H. Ding, C. Yan, W. L. Leong, T. Baikie, Z. Zhang, M. Sherburne, S. Li, M. Asta, N. Mathews and S. G. Mhaisalkar, *Journal of Materials Chemistry A*, 2015, **3**, 23829-23832.
27. T. Yokoyama, D. H. Cao, C. C. Stoumpos, T.-B. Song, Y. Sato, S. Aramaki and M. G. Kanatzidis, *The Journal of Physical Chemistry Letters*, 2016, **7**, 776-782.
28. P. Xu, S. Chen, H.-J. Xiang, X.-G. Gong and S.-H. Wei, *Chemistry of Materials*, 2014, **26**, 6068-6072.
29. C. C. Stoumpos, C. D. Malliakas and M. G. Kanatzidis, *Inorganic Chemistry*, 2013, **52**, 9019-9038.
30. C. C. Stoumpos, L. Frazer, D. J. Clark, Y. S. Kim, S. H. Rhim, A. J. Freeman, J. B. Ketterson, J. I. Jang and M. G. Kanatzidis, *Journal of the American Chemical Society*, 2015, **137**, 6804-6819.
31. M. A. Green, A. Ho-Baillie and H. J. Snaith, *Nature Photonics*, 2014, **8**, 506-514.
32. W.-J. Yin, T. Shi and Y. Yan, *Applied Physics Letters*, 2014, **104**, 063903.
33. M. H. Du, *Journal of Physical Chemistry Letters*, 2015, **6**, 1461-1466.
34. H. Shi and M.-H. Du, *Physical Review B*, 2014, **90**, 174103.
35. J. P. Perdew, K. Burke and M. Ernzerhof, *Physical Review Letters*, 1996, **77**, 3865-3868.
36. A. Alkauskas, P. Broqvist, F. Devynck and A. Pasquarello, *Physical Review Letters*, 2008, **101**, 106802.
37. H.-P. Komsa, P. Broqvist and A. Pasquarello, *Physical Review B*, 2010, **81**, 205118.
38. H.-P. Komsa and A. Pasquarello, *Physical Review B*, 2011, **84**, 075207.
39. S. Lany and A. Zunger, *Physical Review B*, 2008, **78**, 235104.

40. G. Thiele, H. W. Rotter and K. D. Schmidt, *Zeitschrift Fur Anorganische Und Allgemeine Chemie*, 1987, **545**, 148-156.
41. P. E. Blochl, *Physical Review B*, 1994, **50**, 17953-17979.
42. G. Kresse and J. Furthmuller, *Physical Review B*, 1996, **54**, 11169-11186.
43. G. Kresse and D. Joubert, *Physical Review B*, 1999, **59**, 1758-1775.
44. K. Biswas, M. H. Du and D. J. Singh, *Physical Review B*, 2012, **86**, 144108.
45. H. L. Shi and M. H. Du, *Journal of Applied Physics*, 2015, **117**, 175701.
46. D. Yang, W. Ming, H. Shi, L. Zhang and M.-H. Du, *Chemistry of Materials*, 2016, **28**, 4349-4357.
47. N. Onodayamamuro, T. Matsuo and H. Suga, *Journal of Physics and Chemistry of Solids*, 1992, **53**, 935-939.
48. Q. Lin, A. Armin, R. C. R. Nagiri, P. L. Burn and P. Meredith, *Nat Photon*, 2015, **9**, 106-112.
49. J. Even, L. Pedesseau and C. Katan, *The Journal of Physical Chemistry C*, 2014, **118**, 11566-11572.
50. M.-H. Du, *Journal of Applied Physics*, 2010, **108**, 053506.